Journal of Electroanalytical Chemistry 882 (2021) 114992

Contents lists available at ScienceDirect

Journal of Electroanalytical Chemistry

journal homepage: www.elsevier.com/locate/jelechem

# Optimisation of NiO electrodeposition on 3D graphene electrode for electrochemical energy storage using response surface methodology

Elochukwu Stephen Agudosi [a], Ezzat Chan Abdullah [a,*], Arshid Numan [b,c], Mohammad Khalid [c,*], Nabisab Mujawar Mubarak [d,*], Raúl Benages-Vilau [e], Pedro Gómez-Romero [e], Siti Rahmah Aid [f,g], Nurizan Omar [a]

[a] Department of Chemical Process Engineering, Malaysia-Japan International Institute of Technology (MJIIT), Universiti Teknologi Malaysia (UTM), Jalan Sultan Yahya Petra, 54100 Kuala Lumpur, Malaysia
[b] State Key Laboratory of ASIC and System, SIST, Fudan University, 200433 Shanghai, China
[c] Graphene & Advanced 2D Materials Research Group (GAMRG), School of Engineering and Technology, Sunway University, 47500 Petaling Jaya, Selangor, Malaysia
[d] Department of Chemical Engineering, Faculty of Engineering and Science, Curtin University, 98009, Sarawak, Malaysia
[e] Catalan Institute of Nanoscience and Nanotechnology (ICN2), CSIC and The Barcelona Institute of Science and Technology, Campus UAB, E-08193 Bellaterra (Barcelona), Spain
[f] Department of Electronic Systems Engineering, Malaysia-Japan International Institute of Technology (MJIIT), Universiti Teknologi Malaysia (UTM), Jalan Sultan Yahya Petra, 54100 Kuala Lumpur, Malaysia
[g] Graduate School of Information Science and Electrical Engineering, Kyushu University, Fukuoka 819-0395, Japan

ARTICLE INFO

*Article history:*
Received 6 October 2020
Received in revised form 25 November 2020
Accepted 7 January 2021
Available online 19 January 2021

*Keywords:*
Optimization
ANOVA
Electrodeposition
NiO
Binder-free electrode
Energy storage

ABSTRACT

In this study, NiO was electrodeposited on a 3D graphene electrode to produce a nanocomposite with enhanced electrochemical properties. The electrodeposition process parameters such as electrolyte concentration, deposition time, and deposition potential were statistically optimised using response surface methodology. The statistical analysis showed that the optimal electrodeposition conditions to be 0.3 M, 10 min, and -1.2 V for electrolyte concentration, deposition time, and deposition potential, respectively. Furthermore, the predicted model and experimental results for the specific capacity of G-NiO were determined to be 240.91 C/g and 240.58 C/g at 3 mV/s. The results show that the electrochemical deposition technique can be employed as a fast and reliable synthesis route to develop graphene-based metal oxide nanocomposites. The structural and morphological properties were determined by XRD and FESEM studies. The electrochemical measurements revealed the excellent electrochemical performance of 3D graphene NiO composite (G-NiO) for energy storage applications.

## 1. Introduction

The rising need for energy storage systems has continued to increase due to their reliability and portability. Moreover, the depletion of fossil fuel reserves, coupled with their environmental impacts, compels scientists to look for sustainable renewable energy resources and energy storage systems [1]. Lithium-ion batteries, supercapacitors (SCs), and fuel cells, are promising energy storage systems due to their capability to deliver high energy density, high power density, maintain long cycle life as well as being eco-friendly [2,3]. Batteries and SCs are therefore considered as major energy storage devices. Hence, developing devices with a superlative performance to store harvested energy from renewable energy sources are being sought. Batteries can achieve high energy density due to the redox reactions which occur at the electrode surface and internals of the electrodes but are deficient in power density [4]. Thus, SCs have gained tremendous attention and acceptance due to their capabilities to supply high power density, even though they are flawed by low energy density [5]. Considering ecological suitability, supercapacitors have the fast charge-discharge capacity and excellent cyclic efficiency [6].

Therefore, various studies are being carried out to enhance the energy density of SCs without trading off their high power potentiality. Properties that make carbonaceous materials useful as EDLC electrodes are high surface area-to-volume ratio, high electrical and thermal conductivity, excellent thermal and chemical stability, low cost, and eco-friendliness. Typically, carbonaceous materials employ an electrostatic charge storage mechanism and through physical adsorption at the interphase of electrode

* Corresponding authors.
*E-mail addresses:* elochukwuagudosi@gmail.com (E.S. Agudosi), ezzatc@utm.my (E.C. Abdullah), numan.arshed@yahoo.com (A. Numan), khalids@sunway.edu.my (M. Khalid), mubarak.mujawar@curtin.edu.my (N.M. Mubarak), raul.benages@icn2.cat (R. Benages-Vilau), pedro.gomez@icn2.cat (P. Gómez-Romero), sitirahmah.aid@utm.my (S.R. Aid), nurizanomar286@gmail.com (N. Omar).

http://dx.doi.org/10.1016/j.jelechem.2021.114992

and electrolyte yields high power density [7]. Conversely, battery-like materials operate on the principle of redox reactions, which generate high energy density as well as high rate capacity [8]. Nowadays, the production of hybrid electrochemical energy storage systems helps maintain a balance between the properties of batteries and SCs. This kind of energy storage system that aggregates the merits of battery and SC is known as supercapattery.

Redox-active metal oxides such as $Co_3O_4$, $Mn_3O_4$, $Fe_3O_4$, and NiO are employed as electrode materials in enhancing the specific capacity of electrode materials due to their high theoretical specific capacity, good thermal and chemical stability, low price, abundance, and eco-friendliness [9]. Thus, redox-active metal oxides can be supported on carbonaceous materials to improve the materials' electrochemical properties [10]. However, the optimisation of the process parameters that influence electrode materials' specific capacity during their fabrication is imperative. Therefore, the response surface methodology software can be implemented to achieve statistical optimisation for metal oxide thin film growth for electrochemical energy storage applications.

The RSM software is a useful statistical tool deployed in investigating the effects of several variables at different levels, and then, a prediction model with the associated optimum process conditions is generated based on the experimental design [11–13]. Electrodeposition is a multifaceted, cost-effective, fast method of producing nanostructured and functional materials [14] and enables the development of versatile combinations and architectures of electrode materials [15,16]. Electrodeposition of metal oxides is beneficial in that it mitigates the inherent problem associated with active materials support onto inert nanomaterials to achieve excellent material cyclability [17,18]. In the electrodeposition of metal oxides, such parameters as pH, electrolyte concentration, time, potential, applied current density, and agitation are very crucial. The thickness control, composition, and morphology of the deposition films can become more accurate with the proper tuning of these process parameters [19]. It is advantageous to support transition metal oxides on a conductive platform to enhance electrode electro-activity [20]. Three-dimensional (3D) carbon nanostructured electrode materials offer a much larger surface area and render enlarged growth sites for redox-active metal oxides [21,22]. A controlled decoration of carbonaceous material(s) with redox-active metal oxide (s) facilitates rapid charge transport as well as high rate capacity [23]. Some redox-active metal oxides have been supported via electrodeposition on different current collectors such as graphite [24], carbon fibre and papers, nickel dendrites, graphite, and nanoporous gold for energy storage [25]. However, to our knowledge, there is insufficient literature on the parametric optimisation of the electrodeposition of TMOs on substrates for electrochemical energy storage applications.

This study was mainly undertaken to investigate the optimal parametric conditions for NiO thin film's controlled growth on a binder-free graphene electrode (G-Ni) for energy storage applications by implementing the response surface methodology (RSM). The structural features and surface morphology of the fabricated electrode developed under the optimum conditions were determined. Additionally, the electrochemical examination was conducted to measure the fabricated materials' electrochemical performance in a liquid electrolyte.

## 2. Materials and methods

### 2.1. Materials

Nickel foam (thickness of 1.6 mm; bulk density of 0.45 $gcm^{-3}$; and 95% porosity), Potassium hydroxide (KOH), Nickel(II) chloride hexahydrate ($NiCl_2.6H_2O$), Hydrochloric acid (HCl − 37%), ethanol (95%), and acetone (99.5%) were purchased from NA One Solution, Malaysia. The feedstocks were $CH_4$ (99.995%), $H_2$ (99.99%), and Ar (99%) gases and were supplied from NA One Solution, Malaysia. Reagents were of analytical grades and used as received. De-ionised (DI) water was used for all experiments.

### 2.2. Characterisation

The surface morphology and the elemental composition of the developed nanocomposite were analysed using a microscope fitted EDS X-ray detector (JEOL: JSM-7800F). The nanocomposite crystalline nature and phase identification were recorded using a diffractometer (PANalytical-X'Pert MPD) which excites Cu-Kα radiation (wavelength of 1.5418A°) at 0.2/s scan rate; step 0.05° over a 2Θ range of 5° to 90°.

### 2.3. Electrochemical investigations

An electrometer - VersaSTAT-3F model was employed to investigate the developed electrode's electrochemical capability at ambient temperatures. KOH (6 M), a coiled platinum wire, and a saturated calomel electrode were used in a three-electrode system as the electrolyte, counter, and reference electrodes, respectively. Electrochemically, the developed electrodes' properties were determined through cyclic

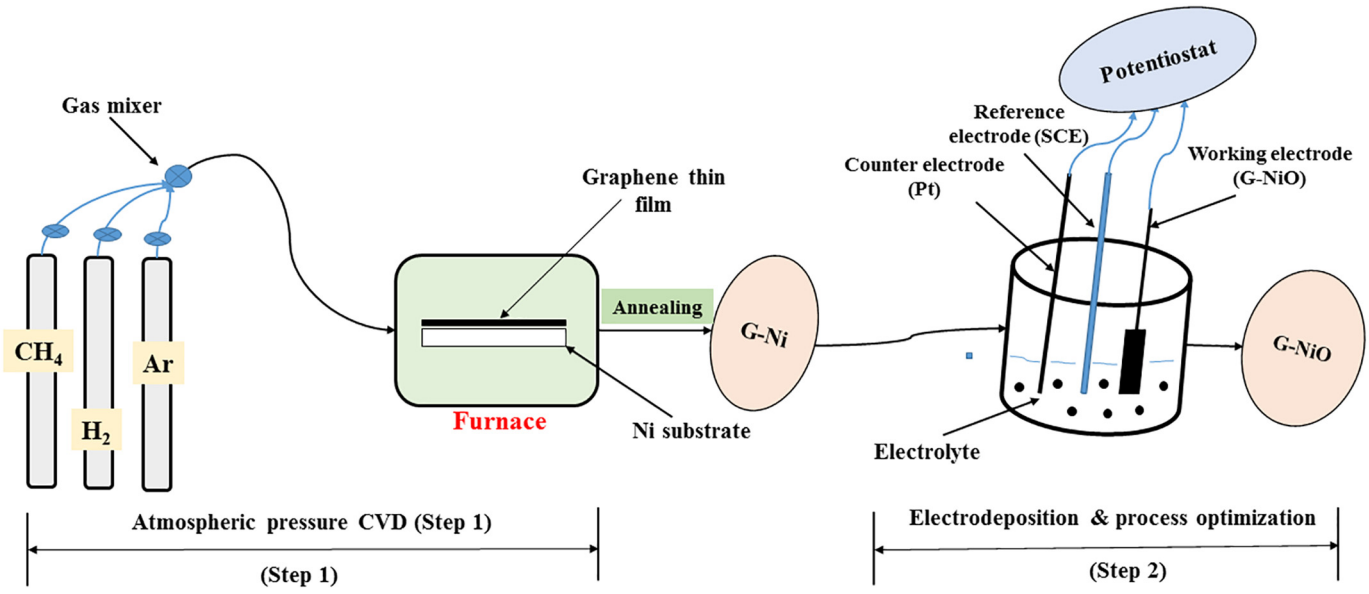


**Fig. 1.** Schematic representation of the two-step route for G-NiO electrode fabrication

**Table 1**
Design factors and coded levels.

| Independent variables | Design factors | Ranges and levels | | |
|---|---|---|---|---|
| | | Low value (−1) | 0 | High value (+1) |
| Electrolyte conc. (°C) | $X_1$ | 0.1 | 0.3 | 0.5 |
| Deposition Time (min) | $X_2$ | 10 | 15 | 20 |
| Deposition Potential (V) | $X_3$ | −1.4 | −1.2 | −1.0 |

voltammetry, galvanostatic charge-discharge, and electrochemical impedance spectroscopy. The CV curve was recorded over a potential window at a specified scan rate, while the charge-discharge properties were evaluated at different current densities. Finally, the impedance measurements were obtained within the frequency range of 0.01 Hz to 100 kHz at an alternating signal of 10 mV (RMS).

### 2.4. Electrodeposition of NiO on graphene electrode

A solution of $NiCl_2.6H_2O$ was used as the electrolyte for depositing NiO on a 3D graphene electrode (G-Ni). G-Ni electrode was prepared through chemical vapour deposition and the electrodeposition took place in a 3-electrode system. The G-Ni electrode was utilised as the working electrode, while a saturated calomel electrode and coiled platinum wire were used as the reference and counter electrodes. Chronoamperometry technique under specified process conditions was employed for the electrodeposition at a constant temperature to deposit NiO on G-Ni electrode. The weight of the G-Ni electrode was measured before electrodeposition. Upon completion of electrodeposition, G-NiO electrode was washed and dried at 80 °C for 12 h in an oven. The dried weight was re-recorded to get the NiO amount deposited on the G-Ni electrode. The developed nanocomposite was labelled as G-NiO electrode. Fig. 1 represents the schematic illustration of the experimental setup for the fabrication of G-NiO electrode.

### 2.5. Experimental design and statistical analysis

Design of experiments (DOE) software - version 12 was used in the design of the experiments. The optimum process conditions for the nanocomposite development were determined and subsequently verified by conducting additional confirmatory experiments. The central composite design (CCD) - an empirical technique of the RSM evaluates the existing relationships between a combination of controlled experimental variables and reports the corresponding responses to the specified criteria [26]. The design was face-centred, with an alpha value of 1.0. The independent variables were chosen and coded as −1 and + 1 at low and high interval levels. Furthermore, the axial points were located at these coordinates: (±α, 0, 0), (0, ±α, 0), (0, 0, ±α), with α being the distance of the axial point from the centre making the design rotatable [27].

The three input parameters deployed in the design of experiments were the electrolyte concentration, deposition time, and deposition potential, while the response was the specific capacity of the fabricated nanocomposite. The levels of these parameters designated as factors $X_1$, $X_2$, and $X_3$ are shown in Table 1. The obtained values of quantitative responses (as designed) for the 17 design factors conducted were arranged in ascending standard order in Table 2. The volume of the electrolyte used for the electrodeposition was kept constant for all experiments. The electrodeposition study was conducted at room temperature. Baş and Boyaci [28] expressed the equation for coding the variables, as stated in Eq. (1).

$$X = \frac{x - [x_{max} + x_{min}]/2}{[x_{max} - x_{min}]/2} \quad (1)$$

where *X, x, $x_{min}$,* and *$x_{max}$* are the coded variable, natural variable, minimum and maximum values of the natural variables, respectively.

Typically, the experimental design establishes several clusters of the independent variables in an arranged manner and lowers the number of experimental runs [29]. In other words, the DOE ensures the experiments are arranged with various combinations of the independent variables (design factors) and thus, reduces the number of experiments to a minimum. According to [30,31], the model correlating the independent variables employs the 2nd degree polynomial function as expressed in Eq. (2).

$$Y = \beta o + \sum_{i=1}^{k} \beta i x i + \sum_{i=1}^{k} \beta i i x i^2 + \sum_{1 \le i \le j}^{k} \beta i j x i x j + \varepsilon \quad (2)$$

where *Y, k, βo, βi, βjj,* and *βij* are the predicted response, number of variables, constant term, coefficient of linear terms, coefficient of quadratic terms, and coefficient of interaction terms, respectively. The terms; *xi* and *xj* are coded design factors. Premkumar and Shanthakumar [32] expressed the model's quantitative form as denoted in Eq. (3).

$$Y = f(X_1, X_2, \ldots\ldots, X_n) \pm \varepsilon \quad (3)$$

where *f* denotes the design response function, *ε* represents errors in the experiment, while *$X_1$, $X_2$, to $X_n$* are independent variables. Moreover, Bas and Boyaci, 2007 [28] expressed the model's matrix code, as stated in Eq. (4).

$$Y = x\beta + \varepsilon \quad (4)$$

The CCD technique was used to develop the correlation between the design factors (electrolyte concentration, deposition time, and deposition potential) while the specific capacity (Qs) was the response. All the 17 experiments were conducted based on the design layout of the independent

**Table 2**
CCD for G-NiO fabrication.

| Std | RUN | Factor 1 A: Electrolyte concentration (M) | Factor 2 B: Deposition time (min) | Factor 3 C: Deposition potential (V) | Response: Specific capacity - $Q_s$ ($Cg^{-1}$) |
|---|---|---|---|---|---|
| 14 | 1 | 0.30 | 10.00 | −1.20 | 240.80 |
| 2 | 2 | 0.10 | 10.00 | −1.00 | 221.40 |
| 15 | 3 | 0.50 | 10.00 | −1.00 | 245.50 |
| 6 | 4 | 0.30 | 15.00 | −1.20 | 243.80 |
| 13 | 5 | 0.10 | 10.00 | −1.40 | 223.40 |
| 11 | 6 | 0.30 | 15.00 | −1.20 | 242.80 |
| 8 | 7 | 0.50 | 10.00 | −1.40 | 262.40 |
| 1 | 8 | 0.30 | 15.00 | −1.00 | 233.50 |
| 16 | 9 | 0.50 | 20.00 | −1.00 | 253.80 |
| 9 | 10 | 0.30 | 20.00 | −1.20 | 245.00 |
| 4 | 11 | 0.50 | 15.00 | −1.20 | 258.20 |
| 10 | 12 | 0.10 | 20.00 | −1.00 | 223.80 |
| 5 | 13 | 0.30 | 15.00 | −1.40 | 242.60 |
| 7 | 14 | 0.10 | 20.00 | −1.40 | 228.70 |
| 12 | 15 | 0.30 | 15.00 | −1.20 | 243.90 |
| 3 | 16 | 0.10 | 15.00 | −1.20 | 225.40 |
| 17 | 17 | 0.50 | 20.00 | −1.40 | 271.5 |

**Table 3**
ANOVA for G-NiO fabrication.

| Source | Sum of squares | DF | Mean square | F value | *P*-value Prob > F | Remark |
|---|---|---|---|---|---|---|
| Model | 3326.91 | 9 | 369.66 | 176.33 | <0.0001 | Significant |
| A – Electrolyte concentration | 2845.97 | 1 | 2845.97 | 1357.53 | <0.0001 | |
| B – Time | 85.85 | 1 | 85.85 | 40.95 | 0.0004 | |
| C – Potential | 256.04 | 1 | 256.04 | 122.13 | <0.0001 | |
| AB | 11.76 | 1 | 11.76 | 5.61 | 0.0497 | |
| AC | 95.91 | 1 | 95.91 | 45.75 | 0.0003 | |
| BC | 1.71 | 1 | 1.71 | 0.8163 | 0.3963 | |
| $A^2$ | 0.6529 | 1 | 0.6529 | 0.3115 | 0.5942 | |
| $B^2$ | 6.80 | 1 | 6.80 | 3.25 | 0.1146 | |
| $C^2$ | 28.41 | 1 | 28.41 | 13.55 | 0.0078 | |
| Residual | 14.68 | 7 | 2.10 | | | |
| Lack of Fit | 13.94 | 5 | 2.79 | 7.53 | 0.1213 | not significant |
| Pure Error | 0.7400 | 2 | 0.3700 | | | |
| Cor Total | 3341.58 | 16 | | | | |

Response, $Q_s$ = Specific capacity.

variables and the responses were recorded accordingly. Moreso, a 2nd order full factorial was implemented for the design factors (three in number) which comprised eight factorial points, six axial points, and three replicates (3 replicates were considered adequate instead of 6 for this study) at the centre points were used and thus, generated 17 experiments altogether according to the expression in Eq. (5) [27].

$$N = 2^n + 2n + nc = 2^3 + 2 \times 3 + 3 = 17 \quad (5)$$

where $N$ and $n$, represent the total number of experiments and the number of factors involved in the experiments, respectively.

## 3. Results and discussions

### 3.1. Statistical optimisation of the NiO electrodeposition

The design of the experiments was done with CCD to determine all the responses for the 17 experimental runs. However, the highest values of the responses determined were not the optimum values for each factor/parameter. The optimised conditions were determined by statically analysing the developed correlation regression model. After the numerical optimisation of the factors (independent variables) was carried out in a separate analysis using the software, the optimum process conditions were determined. Table 2 presents the design layout with the design factors in their various combinations and their quantitative responses. The regression model equation was developed for the specific capacity of the fabricated nanocomposite based on the optimum conditions of the electrodeposition. The experimental data analysis and results validation for the electrodeposition of NiO on the G-Ni electrode was done, and a mathematical model (actual equation) was developed. Again, the DOE software was implemented for the evaluation of ANOVA (analysis of variance).

Table 3 presents the ANOVA results. The F-value of the model (176.33) for the specific capacity, $Q_s$, demonstrates the model's significance. This F-test value is associated with the predicted model's mean squares, which invariably correlate to the residuals' relative mean squares. Similarly, the low values of the Probability > F ($< 0.05$) signify that the regressed model terms are very significant. Conversely, $P$-values $> 0.10$ illustrates non-significant model terms, and this represents a lack of fit for the F-value of 7.53. Thus, the significant model terms recorded were A, B, C, AB, AC, and $C^2$. Besides, the insignificant value for lack of fit indicates the suitability of the model for the electrodeposition of NiO on the G-Ni electrode.

Furthermore, this lack of fit value indicates high efficiency and high model significance model for nanocomposite development. The empirical model developed, which includes the insignificant terms with respect to the responses and the design factors for the specific capacity, $Q_s$, and the model equation is as denoted in Eq. (6).

$$\begin{aligned} Q_s = \; & 120.96 - 45.12X_1 - 2.25X_2 - 187.77X_3 + 1.21X_1X_2 \\ & - 86.56X_1X_3 - 0.46X_2X_3 + 12.34{X_1}^2 + 0.06{X_2}^2 \\ & - 81.41{X_3}^2 \end{aligned} \quad (6)$$

where $Q_s$, $X_1$, $X_2$, and $X_3$ are specific capacity (C/g), electrolyte concentration (M), deposition time (s), and deposition potential (V), respectively.

The developed model's quality was assessed using the value of multiple correlation coefficient ($R^2$) [33]. A good model is predicted as $R^2$ values approach unity (1.00), and this phenomenon signifies that the predicted values correlated well with the values obtained experimentally. The predicted $R^2$ was 0.9766, with an adjusted $R^2$ of 0.9900. The predicted $R^2$ value is in very close conformity with the adjusted $R^2$ value for $Q_s$. Also, the $R^2$ value for specific capacity, $Q_s$ was 0.9956, which shows that the regressed model did not capture only 0.0044% of the discrepancies. Furthermore, a small value of the coefficient of variance was recorded (0.5994% for $Q_s$), which indicates a good accuracy and reliability of the experimental data. Additionally, factors A and C exhibited high model significant values of Prob > F, denoted as 0.0001. The coefficient of the single factor indicates the effect of the constituted factor. Similarly, the coefficient of two factors demonstrates the interaction and the impact of the constituted factors. Hence, from Eq. (6), the positive sign and negative sign in the equation reveal the synergistic effect and antagonistic values of those factors, respectively.

The theoretical values against the experimental values of the developed nanocomposite's specific capacity are shown in Fig. 2. The results revealed that the obtained theoretical values agreed well with the experimental (actual) values, indicating that the model successfully bridged the correlation between the process parameters for the electrode specific capacity value measurements. The residual distribution of the studentised residual against the predicted values can also be used to verify the homogenous variance assumption. Normally distributed errors with clear patterns scattered below and above the straight line demonstrate the residuals' similar nature and indicate that the proposed model is fitted for this study [34].

### 3.2. Surface analysis of NiO electrodeposition

The predicted model's 3D surface response plots illustrate the influence of the independent process variables/factors on the response [33]. The specific capacity over the various combinations of design factors and their relationships are represented on the 3D response surface plots for specific capacity, $Q_s$ in Fig. 3. The effects of specific capacity with independent variables combined with their variables at a fixed level reported different 3D interactive plots. The specific capacity is minimum at low levels of the interactions involving the electrolyte concentration and deposition potential (0.1 M, 10 min, and − 1.4 V). However, there is a region where there is little or no difference in the value of the electrode's specific capacity due to the interactive effects of the factors (with values of the factors at different levels). At this point, the interactive effects of the independent parameters balance out, showing that an optimum value of specific capacity for the different variables exists. From Fig. 3(a), the specific capacity increased as the deposition potential is increased up until the middle levels (at around −1.2 V). However, within the low and middle levels of the electrolyte concentration (between 0.10 M and 0.20 M), the specific capacity is minimal. When the electrolyte concentration is slightly above the middle level, the specific capacity tends to be high in value. With an increase in the deposition potential (a little above −1.3 V and below −1.15 V), more electrons/ions are available to be supported on the 3D graphene electrode causing fast deposition of NiO at a very short time. The curved contour lines depict the interactions between the potential and electrolyte concentration towards the electrode material's electrochemical properties. This demonstrates that the electrolyte concentration and deposition potential

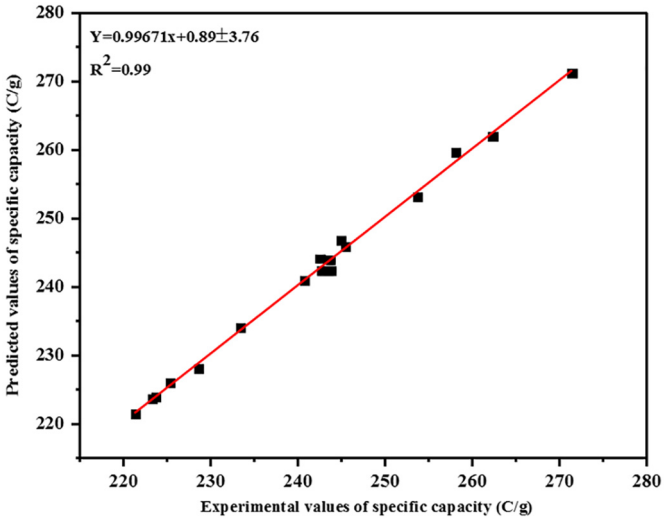


**Fig. 2.** Relationship between the theoretical value and experimental value of the specific capacity.

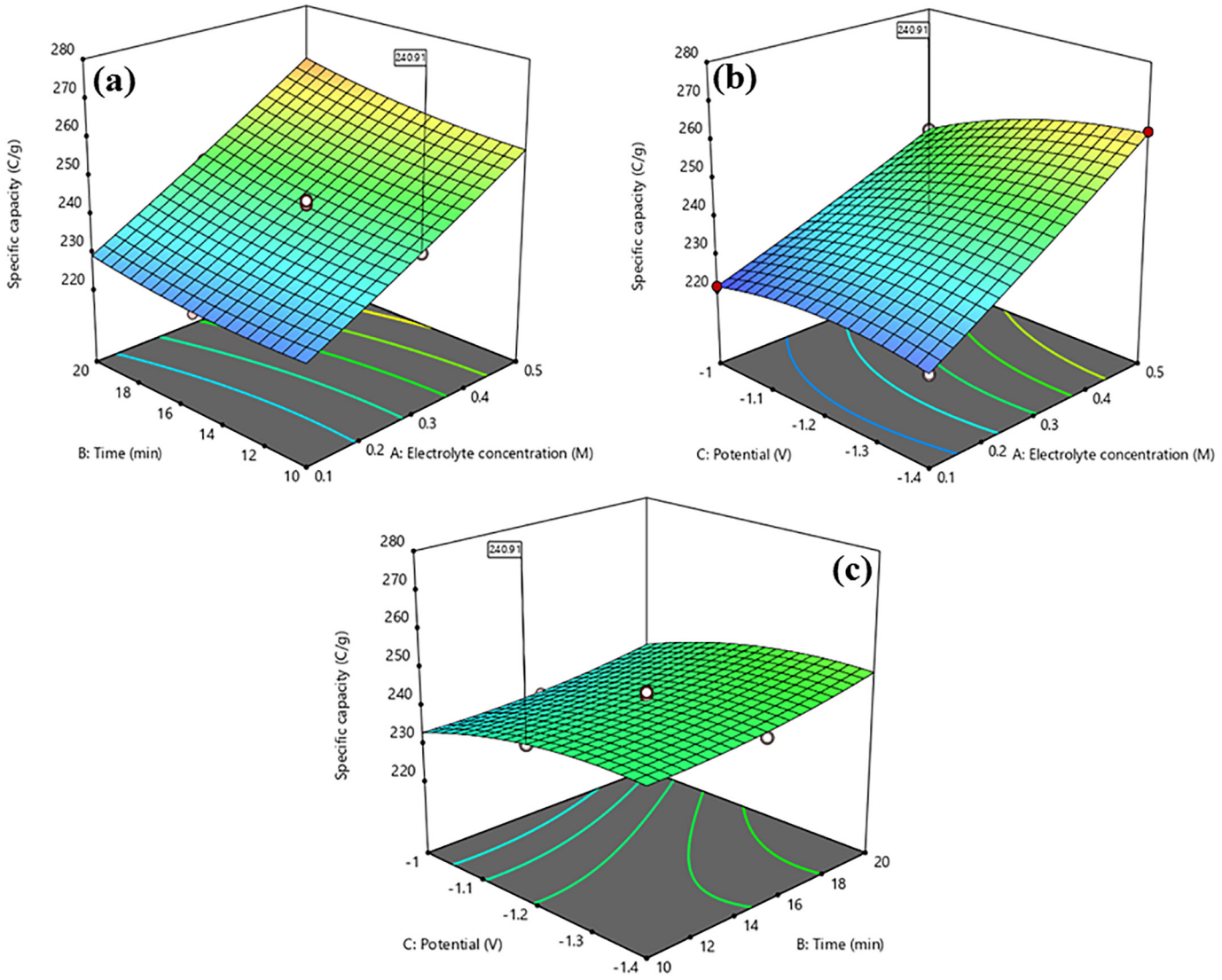


**Fig. 3.** 3D surface plots for the specific capacity using optimised electrodeposition conditions: (a) interactions of deposition time and electrolyte concentration (b) interaction of deposition potential and electrolyte concentration and, (c) interaction of deposition potential and deposition time

effect is very significant in the fabrication of G-NiO electrode with superlative electrochemical performance in aqueous electrolyte.

The highest value of the specific capacity was obtained at levels slightly above the middle point of the deposition potential ( − 1.25 V) with the electrolyte concentration at the middle levels. Moreso, there is a consistency in the effect of deposition time on the electrodeposition with a small decrease in the specific capacity value at the highest and lowest deposition time levels, as shown in Fig. 3(b). There is a little increase in the specific capacity at slightly above the middle and below high levels of both the deposition time and electrolyte concentration ($^{>}$15 min and $^{<}$0.3 M). Furthermore, an increase in the specific capacity value is attained when the deposition time was slightly increased from the low levels. Conversely, there was an increase in specific capacity when the deposition potential was decreased from the high levels, as shown in Fig. 3(c). Likewise, the same results are seen with the deposition potential interactive effect on the electrode electrochemical properties but with a stronger perturbation as illustrated in Fig. 4.

The interactions of the variables between the electrolyte concentration as an independent variable are extremely significant when $P < 0.0001$. The evaluation of the regression model significance and ANOVA results demonstrate the associated performances which are well illustrated by the apex points of the contour lines. Thus, these results reveal the satisfactory description of the model by the range of the experimental factors studied. The fitted regression equation showed a good model fit and expressed the correlation between the independent variables (design factors) demonstrated by similar studies [31,35,36].

### 3.3. Perturbation effect on specific capacity

Process factors such as the electrolyte concentration, time, and deposition potential influence the specific capacity of the developed nanocomposite. The optimisation goal was to predict a response using the quadratic model and thereafter, validate it statistically through the observed experimental data. The optimum experimental conditions were identified through the generated design contour maps. The three design factors denoted as A, B, and C could be taken as the axes in generating the contour maps. The most sensitive factors to the response were chosen by employing the perturbation plots. All the three factors were plotted on one response graph to generate the perturbation plots. From a reference point, these plots demonstrate each factor's effect over its range on the response. Perturbation plots display the effect of a factor over its window while keeping other factors at constant points within the design space. The response graph is plotted with one factor being varied within its window while keeping all other factor positions constant.

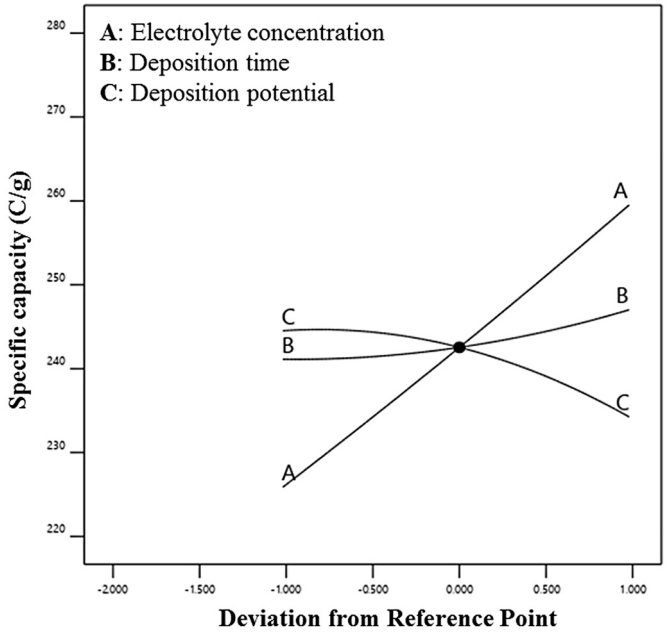


**Fig. 4.** Effect of perturbation plot for G-NiO fabrication.

The response (specific capacity) was plotted over the deviations from the reference point with the interactive effects of all other factors within its range, as illustrated in Fig. 4. Perturbation plots revealed that good interactions existed between all the three factors in the design. However, the perturbation of deposition potential (C) of the variance at around −1.29 V gave a very significant electrochemical performance up to 99.9% in aqueous solution (6 M KOH). Similarly, the electrolyte concentration (factor A) and deposition time (factor B) of the electrodeposition do have strong effects with factor B showing more influence but not as powerful as the deposition potential on the specific capacity when the perturbation is given in the statistical analysis. Therefore, the response (specific capacity) showed more sensitivity to variations in factors A and C than B. The plots' pattern for all three independent variables reveals that the specific capacity is responsive to all the variables for electrodeposition [37–39].

### 3.4. Optimisation of electrodeposition and model verification

Upon the statistical optimisation of NiO's electrodeposition conditions on the 3D graphene electrode, the optimum values were obtained for the predicted model. The validation of the developed model was carried out by carrying out additional experiments with the predicted optimised values of the process conditions for NiO growth. The model predicted optimised values were 240.91 C/g, 0.30 M, 10 min, and − 1.20 V for specific capacity, electrolyte concentration, deposition time, and deposition potential, respectively. After performing additional experiments, a reasonable difference (of 0.33 C/g only) was realised between the experimental data and predicted values of the model. Thus, the model is adjudged the best fit to the experimental data. Additionally, the software's optimisation analysis delivered the best as selected based on the responses fed to the software. Drawing the model's surface plots enables good visualisation of the effect of design factors on the responses [30]. The specific capacity ($Q_s$), obtained over various combinations of variables and their interactions are represented on the 3D response surface plots in Fig. 3.

The high specific capacity of the fabricated nanocomposite was achieved due to the remarkable electrochemical performance. This superlattice performance resulted from the structural and morphological properties of the electrode material. To assess the predicted model's validity, additional experiments were carried out using the optimal conditions for the optimised specific capacity to verify and validate the predicted values. With the optimum electrodeposition conditions, three different additional experiments were conducted to validate the predicted model. Hence, the predicted model and experimental results for the response (specific capacity) obtained to validate the model were 240.91 C/g and 240.58 C/g, respectively. With only a 0.14% difference obtained from the experimental results, the model is well fitted.

### 3.5. Structural and morphological analysis

The phase purity, structure, and morphology of G-NiO electrode developed at the optimum electrodeposition conditions were studied through XRD and FESEM-EDS studies. XRD determines the crystallographic structure of the graphene electrode. XRD patterns were obtained over 2Θ range from 5° to 90° with monochromatised Cu K-α radiation. Fig. 5(a)-(b) displays the XRD patterns of the (3D) graphene electrode (G-Ni) and G-NiO with lattice parameters of (002) at 26.45° (111) at 44.51°, (200) at 51.85°, and (220) at 76.37°. The difference in the structure is evident from their intensities. The XRD peaks for Ni, G-Ni and G-NiO could be matched as the NiO cubic crystal phase and peaks are well sharped and documented (JCPDS card Nos: 22–1189 and 73–1523) [40] and (JCPDS card Nos: 87–0712 and 47–1049) [41]. A unique peak was seen in the graphene deposited nickel foam at a 2 theta peak position of 26.45°, confirming graphene presence [42]. These crystallographic characteristics of the carbon atoms formed the building block for the enhanced electro-activity of the nanocomposite due to its conductive nature and strong bonding (adhesion) to both the nickel substrate and NiO thin film. In the deposited NiO thin film onto the graphene film, homogenous oxide layers are formed without any apparent impurities. With the CCD optimisation, a further microscopic study on the formation and structure of the G-NiO developed at the optimum conditions reveals the sheet and distinctive sea urchin-like shape of the NiO thin film as evidenced in Fig. 5(c). This unique morphological property of the NiO plays a synergistic role in the nanocomposite which boosts the electro-active capability of the electrode in aqueous electrolytes for energy storage. On the contrarily, Fig. 5(d) portrays the non-uniformity like the urchin-like shape of the nanocomposite obtained without CCD optimisation and resulted in low electrode electrochemical performance. Fig. 5(e) depicts the EDS results of the G-NiO prepared using the CCD optimum conditions of the electrodeposition parameters; inset of Fig. 5 (e) displays the atomic percentages of the associated elements.

### 3.6. Cyclic voltammetry

The cyclic voltammetric (CV) responses of G-NiO electrode prepared at the optimum electrodeposition conditions were measured over the potential window of 0.6 V at different scan rates of 3–50 mV/s in a standard 3-electrode cell at 25 °C. From Fig. 6(a), the CV curves show well-defined redox peaks indicating the behaviour of a battery-grade material. The peaks indicate the redox transformation of Ni ionic species due to the Nernstian process (non-capacitive faradaic behaviour). The generated symmetric redox peaks can be ascribed to the migration and diffusion of ionic species as the electrolyte is dispersed, suggesting that NiO is exhibiting battery-type characteristics [43]. The NiO electrode redox behaviour is based on a non-faradaic redox mechanism, as demonstrated by the symmetric CV curves. At a low scan rate, the hydroxyl ions had ample time to be dispersed in the electrode which gave higher specific capacity whereas, at a high scan rate, electrolyte ions had less time to diffuse and intercalate into the electrode resulting in a lower specific capacity [44]. The redox peaks show the excellent reversible behaviour of the material. Also, it could be observed that an increase in the CV scan rate increases the redox peak current of the electrode showing high rate capability and better reversibility [45].

In Fig. 6(b), the comparative CV curves of NiO and G-NiO electrodes at the same scan rates of 3 mV/s and 10 mV/s demonstrate the great influence of graphene as the specific capacity of the electrode is drastically improved. The electrochemical performance of G-NiO electrode was greatly enhanced due to the presence of graphene, unlike the NiO electrode without

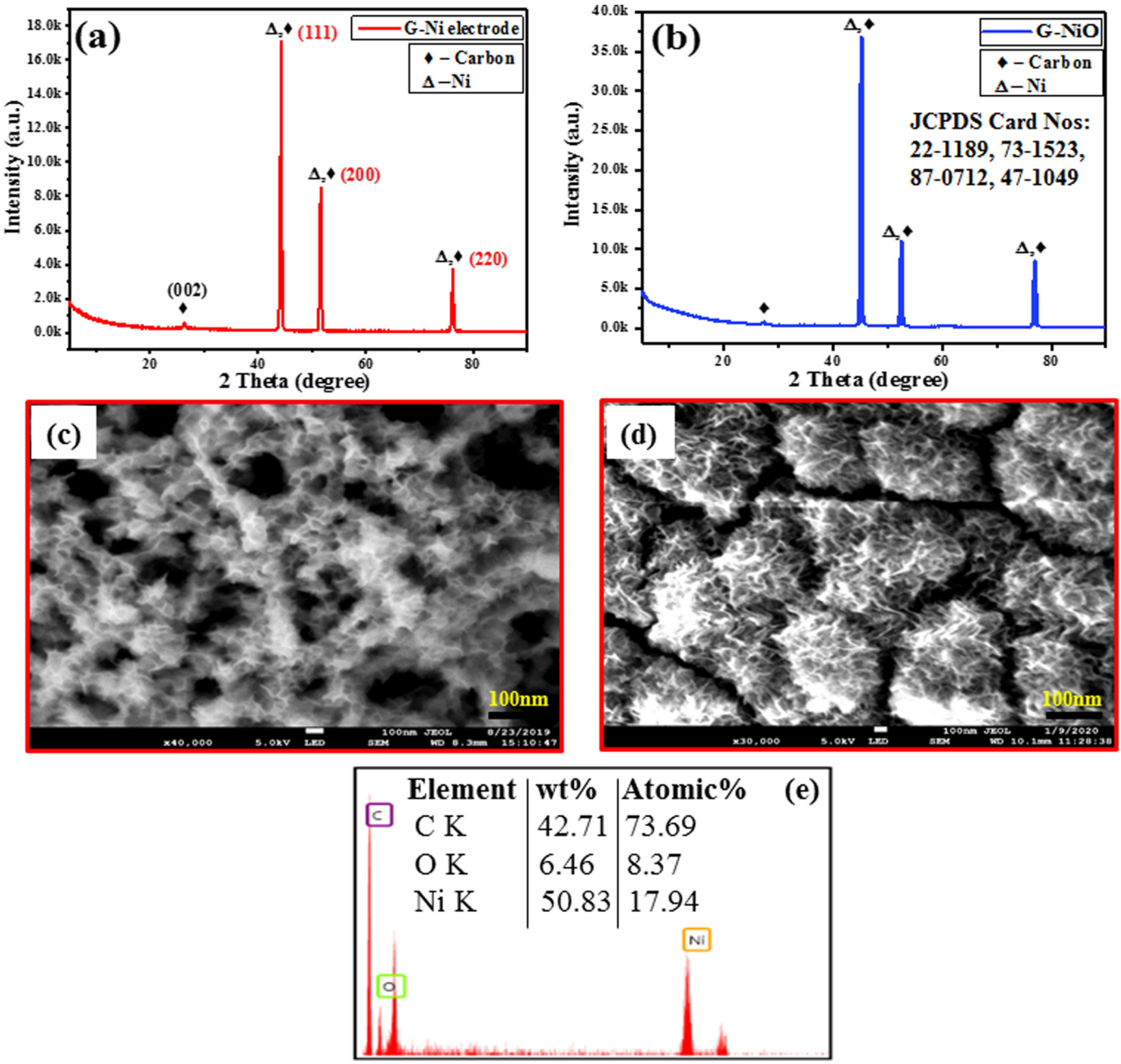


**Fig. 5.** (a) XRD spectrum of 3D graphene electrode, (b) XRD spectrum of G-NiO based on CCD optimisation, (c) FESEM image of G-NiO based on CCD optimisation, (d) FESEM image of G-NiO without optimisation, and (e) EDS spectrum of the G-NiO with optimisation

graphene. Moreover, the presence of graphene in the nanocomposite enhanced the redox peak current leading to a significant increase in the electrode performance with better reversibility. Additionally, graphene's presence significantly improved the disclosure of the electrode's available active sites for redox reactions due to the larger surface area and its conductive platform (high electrical conductivity). The G-NiO electrode exhibited a higher and remarkable peak current owing to the high surface area of graphene compared to NiO electrode. This phenomenon brought about improved electrochemical performance of the G-NiO electrode. The high background current for G-NiO electrode compared to NiO electrode is as a result of the highly conductive platform of the graphene in the hybrid G-NiO composite. Also, the amorphous phase, which was generated from the graphene and NiO structures enhances electro-activity. Therefore, the combination of NiO and graphene improved the material (G-NiO) conductivity, rate capability, reversibility, and cyclic stability.

The value of the specific capacity of G-NiO electrode prepared at the optimum electrodeposition conditions was measured to be 240.58 C/g. In comparison, the NiO electrode delivered 115.52 C/g under the same optimal conditions by using the relation as expressed in Eq. (7).

$$Q_s = \frac{1}{v \times m} \int_{V_i}^{V_f} I \times (V) dV \ (\mathrm{CV}) \tag{7}$$

where *v, V, I,* and *m* are the scan rate, operating potential, current, and mass of active materials, respectively. The region under the oxidation-reduction peaks is represented by the integral term.

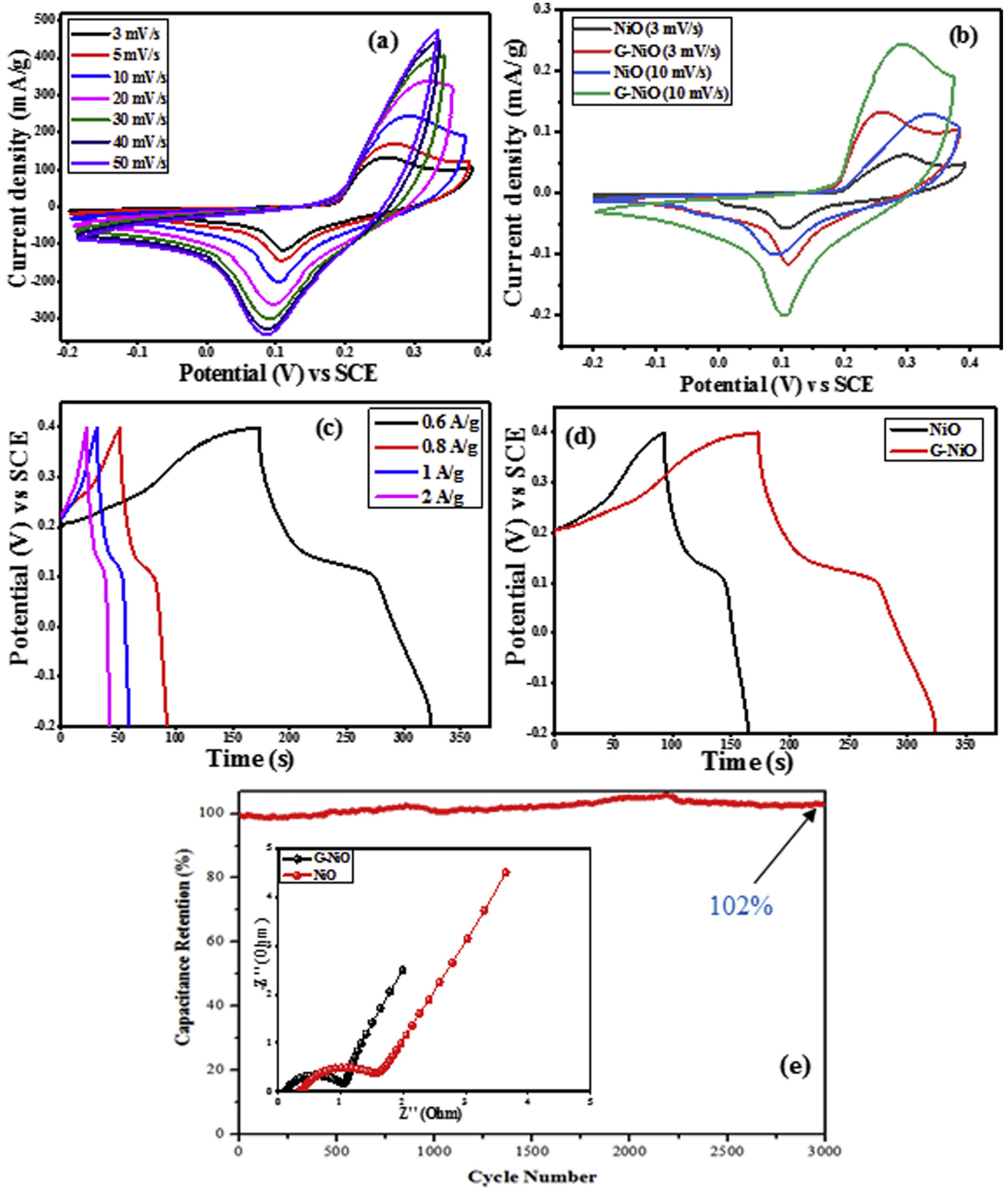


**Fig. 6.** (a) CV curve of G-NiO electrode at different scan rates, (b) comparative CV curves of NiO and G-NIO electrodes at the same scan rates of 3 mV/s and 10 mV/s, (c) GCD plots of G-NiO electrode at different current densities, (d) comparative GCD plots of NiO and G-NIO electrodes at the same current density (0.6 A/g), and (e) cyclic stability performance of G-NiO electrode showing the excellent cyclability; inset depicts the EIS spectrum of the fabricated G-NiO electrode at the optimised electrodeposition conditions

### 3.7. Galvanostatic charge-discharge tests

The galvanostatic charge-discharge (GCD) measurements were conducted to further probe into G-NiO electrode's electrochemical performance. The electrode's battery-grade properties are well demonstrated from the GCD plots based on the Nernstian process. Fig. 6(c) represents the GCD plots for G-NiO electrode prepared under optimum electrodeposition conditions. The GCD characteristics were determined different current densities over a potential range of 0.6 V at room temperature. The G-NiO electrode's specific capacity measured from the GCD plot at 0.6 A/g was 91.67 C/g according to the relation as in Eq. (8).

$$Q_s = \frac{I \times t}{m}\ (\mathrm{GCD}) \tag{8}$$

where $I$, $m$, and $\Delta t$ are the discharge current, mass of active materials, and discharge time reported for a complete discharge, respectively.

Fig. 6(d) shows the comparative GCD plots of NiO and G-NiO electrode illustrating the effect of graphene. Similar to the CV measurements, at lower current density higher charge storage capacity of the electrode is achieved and vice versa. In comparison with previous studies that have demonstrated the performance of redox-active metal oxides as electrode materials, the reported specific capacity of G-NiO is significantly higher based on present study conditions [46,47]. The GCD plots show that the specific capacity is very significant at the optimum electrodeposition conditions. This effect is due to the best combinations of the process parameters, which gives an excellent interactive effect in electrochemical energy storage. Furthermore, the 3D nano-architecture of G-NiO electrode contributes positively towards the fast migration and transport of ions into the electrode and hence, minimises the activation energy of the ionic species [48,49].

Additionally, a hybrid composite of graphene and NiO produces a significant electrochemical performance due to the conductive platform provided by graphene as well as the synergistic effect of NiO. The linear nature of the relationship between the specific capacity and surface area could be seen as demonstrated in the related studies that utilised such materials as NiO [50] and carbon [51] for energy storage application. A larger current provides more active sites and environments to generate a larger number of redox reactions due to the electrode material's larger surface area. In effect, sizeable current tolerance during the charge-discharge process shows good redox-active material behaviour, leading to high energy density [52].

### 3.8. Electrochemical impedance spectroscopy measurements

The charge storage kinetics investigation of the fabricated electrode (G-NiO) with the optimum electrodeposition conditions, was conducted in a potentiostatic mode. Essentially, Electrochemical Impedance Spectroscopy (EIS) deals with the mechanism of the migration and dispersion of reactants to and/or away from the electrode surface, which produces a particular frequency character known as “Warburg impedance” [53]. The diffusion resistance is measured from the slope in the low-frequency area of the Warburg impedance. The impedance can reveal the electrochemical characteristics of electrode materials. Inset of Fig. 6(e) depicts the EIS spectra of NiO electrode and the developed G-NiO electrode at the optimum electrodeposition conditions. Each spectrum comprises a typical semicircle and an adjoining straight line. A semicircle in the frequency character is characteristic of the charge transfer resistance occurring at the electrode and electrolyte interface [54]. The material behaviour in the high-frequency and low-frequency regions is signified by a semicircle and a straight line, respectively. The electrode capacitive behaviour is represented by a straight line at the low-frequency region.

From the Nyquist plots, it could be observed that NiO and G-NiO electrodes portray the impedance behaviour by showing a frequency character with a straight line at the low-frequency region demonstrating the battery-like characteristics of the materials with G-NiO having a lower charge transfer resistance ($R_{ct}$ = 0.17 Ω) than NiO electrode ($R_{ct}$ = 0.46 Ω). A bigger semicircle of the Warburg impedance (high-frequency region) reveals a higher charge transfer resistance of the electrode material. In principle, three factors are crucial in measuring the electrode resistance. They include: (a) the lack of continuity in the electric conductivity and ionic conductivity, which occurs during the charge transfer process, (b) the resistance between the electron collector (NF) and leads (connectors), and (c) the resistance (intrinsic) of the electron collector [55]. It could be seen from the plot that G-NiO electrode recorded a straight line parallel to the imaginary axis ($Z_{im}$) and hence, proves an adequate charge storage capacity due to high conductivity. This further demonstrates that G-NiO electrode has a uniform oxide layer of NiO supported on the 3D graphene electrode. By implication, controlled NiO thin film deposition on graphene thin film produces an amorphous phase of the composite, which is considered highly conductive. The unique properties of the nanocomposite (G-NiO) aids in reducing the pathway for the transportation/migration of ions to the nickel foam (electron collector) and results in the enhanced performance of the electrode, making it an excellent candidate for energy storage in various utilisations.

The evaluation of the G-NiO electrode's viability in electrochemical energy storage application was conducted through a cyclic stability study. The developed electrode was subjected to a prolonged charge-discharge of 3000 cycles for this purpose. Fig. 6(e) is the cyclic stability performance of G-NiO electrode, showing an excellent result of 102% specific capacitance retention after 3000 cycles. The stability test shows that the electrode's activation process in the aqueous electrolyte was stable with a continuous initial slight increase in specific capacity until the 900th cycle, where the value was about 102%. The specific capacitance value was then slightly decreased (100.5%) and then increased (102%) until the 2000th cycle. This increment continued to about 104% at the 2250th cycle and then gradually decreased to 102% until the 3000th cycle. As proven by the cyclic stability performance, this excellent cyclability of the electrode presents the G-NiO as a potential electrode candidate for electrochemical energy storage application.

## 4. Conclusions

The electrochemical performance measurements of the graphene-based nanocomposite (G-NiO) developed via electrochemical deposition method were investigated for energy storage applications. The statistical analysis revealed that the electrodeposition variables' optimised values at room temperature were 0.30 M, 10 min, and − 1.20 V for electrolyte concentration, deposition time, and deposition potential, respectively. Moreover, the effect of the residuals was non-significant, and the predicted $R^2$ value tallied well with the adjusted $R^2$ value for the response, $R$. These results demonstrate the validity and fitting of the developed model for the process behaviour forecast. The XRD and FESEM-EDS analyses indicate that the composition of NiO thin film and graphene thin film reported an amorphous phase of uniformly distributed thin films. Furthermore, the results of the electrochemical measurements of the developed nanocomposite were 240.58C/g at 3 mV/s, 91.67 C/g at 0.6 A/g, and $R_{ct}$ of 0.17 Ω. Thus, the results reveal the battery-like features of the fabricated binder-free nanocomposite and its promising potentials to be utilised as electrode material in developing electrochemical energy storage systems.

## Funding

This work was supported by Malaysia-Japan International Institute of Technology (MJIIT) of Universiti Teknologi Malaysia and MJIIT JICA Fund [UTM-Vot: 4B593].

## Authorship statement

All persons who meet authorship criteria are listed as authors, and all authors certify that they have participated sufficiently in work to

take public responsibility for the content, including participation in the concept, design, analysis, writing, or revision of the manuscript. Furthermore, each author certifies that this material or similar material has not been and will not be submitted to or published in any other publication.

## Declaration of Competing Interest

No competing interests amongst the authors.

## References


[1] A.E. Elkholy, F. El-Taib Heakal, N.K. Allam, A facile electrosynthesis approach of amorphous Mn-co-Fe ternary hydroxides as binder-free active electrode materials for high-performance supercapacitors, Electrochim. Acta 296 (2019) 59–68.

[2] B. Yao, S. Chandrasekaran, J. Zhang, W. Xiao, F. Qian, C. Zhu, E.B. Duoss, C.M. Spadaccini, M.A. Worsley, Y. Li, Efficient 3D printed Pseudocapacitive electrodes with ultrahigh $MnO_2$ loading, Joule 3 (2) (2019) 459–470.

[3] G. Zhao, C. Chen, D. Yu, L. Sun, C. Yang, H. Zhang, Y. Sun, F. Besenbacher, M. Yu, One-step production of O-N-S co-doped three-dimensional hierarchical porous carbons for high-performance supercapacitors, Nano Energy 47 (2018) 547–555.

[4] Z. Wu, L. Li, J.-m. Yan, X.-b. Zhang, Materials design and system construction for conventional and new-concept supercapacitors, Adv. Sci. 4 (6) (2017) 1600382.

[5] A. Yu, V. Chabot, J. Zhang, Electrochemical Supercapacitors for Energy Storage and Delivery: Fundamentals and Applications, 2017.

[6] A. Burke, Ultracapacitors: why, how, and where is the technology, J. Power Sources 91 (1) (2000) 37–50.

[7] S. Najib, E. Erdem, Current progress achieved in novel materials for supercapacitor electrodes: mini review, Nanoscale Adv. 1 (8) (2019) 2817–2827.

[8] H. Shao, N. Padmanathan, D. McNulty, C. O'Dwyer, K.M. Razeeb, Supercapattery based on binder-free $Co_3(PO_4)_2{\cdot}8H_2O$ multilayer nano/microflakes on nickel foam, ACS Appl. Mater. Interfaces 8 (42) (2016) 28592–28598.

[9] R.S. Kate, S.A. Khalate, R.J. Deokate, Overview of nanostructured metal oxides and pure nickel oxide (NiO) electrodes for supercapacitors: a review, J. Alloys Compd. 734 (2018) 89–111.

[10] G. Wang, L. Zhang, J. Zhang, A review of electrode materials for electrochemical supercapacitors, Chem. Soc. Rev. 41 (2) (2012) 797–828.

[11] K. Silas, W.A.W. Ab Karim Ghani, T.S.Y. Choong, U. Rashid, Optimization of activated carbon monolith $Co_3O_4$-based catalyst for simultaneous $SO_2$/NOx removal from flue gas using response surface methodology, Combust. Sci. Technol. (2019) 1–18.

[12] N.A.A. Talib, F. Salam, N.A. Yusof, S.A. Alang Ahmad, Y. Sulaiman, Modeling and optimization of electrode modified with poly(3,4-ethylenedioxythiophene)/graphene oxide composite by response surface methodology/box-Behnken design approach, J. Electroanal. Chem. 787 (2017) 1–10.

[13] M. Li, C. Feng, Z. Zhang, X. Liu, W. Ma, Q. Xue, N. Sugiura, Optimization of electrochemical ammonia removal using box–Behnken design, J. Electroanal. Chem. 657 (1) (2011) 66–73.

[14] D. Lincot, Solution growth of functional zinc oxide films and nanostructures, MRS Bull. 35 (10) (2010) 778–789.

[15] D. Zhu, C. Xia, Z. Yang, T. Yang, Q. Li, R. Liu, Fast electrodeposition of Ni/$Ni(OH)_2$ nanoparticles on nanoporous cu prepared by dealloying Zr-Cu amorphous alloy for supercapacitor application, Electrochim. Acta 334 (2020) 135591.

[16] A. Toghraei, T. Shahrabi, G. Barati Darband, Electrodeposition of self-supported Ni-Mo-P film on Ni foam as an affordable and high-performance electrocatalyst toward hydrogen evolution reaction, Electrochim. Acta 335 (2020) 135643.

[17] G.Z. Chen, Supercapacitor and supercapattery as emerging electrochemical energy stores, Int. Mater. Rev. 62 (4) (2017) 173–202.

[18] T. Nguyen, M. Boudard, M.J. Carmezim, M.F. Montemor, Layered $Ni(OH)_2$-$Co(OH)_2$ films prepared by electrodeposition as charge storage electrodes for hybrid supercapacitors, Sci. Rep. 7 (1) (2017) 39980.

[19] G. Lima, J. Braga, G. Gozzi, L. Fugikawa-Santos, Optimization of the electrical performance of metal oxide thin-film transistors by varying spray deposition parameters, MRS Adv. 3 (2018) 1–7.

[20] J.-H. Jeong, J.W. Park, D.W. Lee, R.H. Baughman, S.J. Kim, Electrodeposition of α-$MnO_2$/γ-$MnO_2$ on carbon nanotube for yarn supercapacitor, Sci. Rep. 9 (1) (2019) 11271.

[21] D.P. Dubal, P. Gomez-Romero, B.R. Sankapal, R. Holze, Nickel cobaltite as an emerging material for supercapacitors: an overview, Nano Energy 11 (2015) 377–399.

[22] E.S. Agudosi, E.C. Abdullah, A. Numan, N.M. Mubarak, S.R. Aid, R. Benages-Vilau, P. Gómez-Romero, M. Khalid, N. Omar, Fabrication of 3D binder-free graphene NiO electrode for highly stable supercapattery, Sci. Rep. 10 (1) (2020) 11214.

[23] D. Zhang, Y. Shao, X. Kong, M. Jiang, X. Lei, Hierarchical carbon-decorated $Fe_3O_4$ on hollow CuO nanotube array: fabrication and used as negative material for ultrahigh-energy density hybrid supercapacitor, Chem. Eng. J. 349 (2018) 491–499.

[24] J. Ni, H. Wang, Y. Qu, L. Gao, $PbO_2$ electrodeposited on graphite for hybrid supercapacitor applications, Phys. Scr. 87 (4) (2013), 045802, .

[25] M. Montemor, S. Eugénio, N. Tuyen, R. Silva, T. Moura e Silva, M. Carmezim, Nanostructured Transition Metal Oxides Produced by Electrodeposition for Application as Redox Electrodes for Supercapacitors, 2016 681–714.

[26] F. Ghorbani, H. Younesi, S.M. Ghasempouri, A.A. Zinatizadeh, M. Amini, A. Daneshi, Application of response surface methodology for optimization of cadmium biosorption in an aqueous solution by *Saccharomyces cerevisiae*, Chem. Eng. J. 145 (2) (2008) 267–275.

[27] I.A.W. Tan, A.L. Ahmad, B.H. Hameed, Optimization of preparation conditions for activated carbons from coconut husk using response surface methodology, Chem. Eng. J. 137 (3) (2008) 462–470.

[28] D. Baş, İ.H. Boyacı, Modeling and optimization I: usability of response surface methodology, J. Food Eng. 78 (3) (2007) 836–845.

[29] H. Kalavathy, I. Regupathi, M.G. Pillai, L.R. Miranda, Modelling, analysis and optimization of adsorption parameters for H3PO4 activated rubber wood sawdust using response surface methodology (RSM), Colloids Surf. B: Biointerfaces 70 (1) (2009) 35–45.

[30] B.W.B. Kueh, S. Yusup, N. Osman, Supercritical carbon dioxide extraction of *Melaleuca cajuputi* leaves for herbicides allelopathy: optimization and kinetics modelling, J. CO2 Utilizat. 24 (2018) 220–227.

[31] M.A. Bezerra, R.E. Santelli, E.P. Oliveira, L.S. Villar, L.A. Escaleira, Response surface methodology (RSM) as a tool for optimization in analytical chemistry, Talanta 76 (5) (2008) 965–977.

[32] M. Premkumar, S. Shanthakumar, Process optimization for Cr(VI) removal by *Mangifera Indica* seed powder: a response surface methodology approach, Desalin. Water Treat. 53 (6) (2015) 1653–1663.

[33] B. Liu, J. Peng, L. Zhang, R. Wan, S. Guo, L. Zhou, Optimization of preparation for $Co_3O_4$ by calcination from cobalt oxalate using response surface methodology, Chem. Eng. Res. Des. 88 (8) (2010) 971–976.

[34] R. Singh, R. Chadetrik, R. Kumar, K. Bishnoi, D. Bhatia, A. Kumar, N.R. Bishnoi, N. Singh, Biosorption optimization of lead(II), cadmium(II) and copper(II) using response surface methodology and applicability in isotherms and thermodynamics modeling, J. Hazard. Mater. 174 (1) (2010) 623–634.

[35] M.İ. Coşkun, İ.H. Karahan, Y. Yücel, T.D. Golden, Modeling the effect of temperature and potential on the in vitro corrosion performance of biomedical hydroxyapatite coatings, Metall. Mater. Trans. A 47 (10) (2016) 5169–5180.

[36] P.R. Jagadish, M. Khalid, N. Amin, L.P. Li, A. Chan, Process optimisation for n-type $Bi_2Te_3$ films electrodeposited on flexible recycled carbon fibre using response surface methodology, J. Mater. Sci. 52 (19) (2017) 11467–11481.

[37] S.H. Hashemi, M. Montazer, N. Naghdi, T. Toliyat, Formulation and characterization of alprazolam-loaded nanoliposomes: screening of process variables and optimizing characteristics using RSM, Drug Dev. Ind. Pharm. 44 (2) (2018) 296–305.

[38] B. Sadhukhan, N.K. Mondal, S. Chattoraj, Optimisation using central composite design (CCD) and the desirability function for sorption of methylene blue from aqueous solution onto Lemna major, Karbala Int. J. Mod. Sci. 2 (3) (2016) 145–155.

[39] M.T.H. Siddiqui, S. Nizamuddin, N.M. Mubarak, K. Shirin, M. Aijaz, M. Hussain, H.A. Baloch, Characterization and process optimization of biochar produced using novel biomass, waste pomegranate peel: a response surface methodology approach, Waste Biomass Valoriz. 10 (3) (2019) 521–532.

[40] D. Mohammadyani, S.A. Hosseini, S.K. Sadrnezhaad, Characterization of nickel oxide nanoparticles synthesized via rapid microwave-assisted route, Int. J. Mod. Phys. Conf. Series 05 (2012) 270–276.

[41] L.G. Teoh, K.-D. Li, Synthesis and characterization of NiO nanoparticles by sol– gel method, Mater. Trans. 53 (12) (2012) 2135–2140.

[42] S. Das, M. Kim, J.W. Lee, W. Choi, Synthesis, properties, and applications of 2-D materials: a comprehensive review, Critic. Rev. Solid State Mater. Sci. 39 (4) (2014) 231–252.

[43] Q. Li, J. Zhou, R. Liu, L. Han, An amino-functionalized metal–organic framework nanosheet array as a battery-type electrode for an advanced supercapattery, Dalton Trans. 48 (46) (2019) 17163–17168.

[44] N. Duraisamy, A. Numan, K. Ramesh, K.-H. Choi, S. Ramesh, S. Ramesh, Investigation on structural and electrochemical properties of binder free nanostructured nickel oxide thin film, Mater. Lett. 161 (2015) 694–697.

[45] N. Duraisamy, N. Arshid, K. Kandiah, J. Iqbal, P. Arunachalam, G. Dhanaraj, K. Ramesh, S. Ramesh, Development of asymmetric device using $Co_3(PO_4)_2$ as a positive electrode for energy storage application, J. Mater. Sci. Mater. Electron. 30 (8) (2019) 7435–7446.

[46] P. Bhattacharya, T. Joo, M. Kota, H.S. Park, CoO nanoparticles deposited on 3D macroporous ozonized RGO networks for high rate capability and ultralong cyclability of pseudocapacitors, Ceram. Int. 44 (1) (2018) 980–987.

[47] E.S. Agudosi, E.C. Abdullah, A. Numan, N.M. Mubarak, M. Khalid, N. Omar, A review of the graphene synthesis routes and its applications in electrochemical energy storage, Critic. Rev. Solid State Mater. Sci. (2019) 1–39.

[48] N. Balke, S. Kalnaus, N.J. Dudney, C. Daniel, S. Jesse, S.V. Kalinin, Local detection of activation energy for ionic transport in Lithium cobalt oxide, Nano Lett. 12 (7) (2012) 3399–3403.

[49] S. Aderyani, P. Flouda, J.L. Lutkenhaus, H. Ardebili, The effect of nanoscale architecture on ionic diffusion in rGo/aramid nanofiber structural electrodes, J. Appl. Phys. 125 (18) (2019) 185106.

[50] H. Pang, Y. Shi, J. Du, Y. Ma, G. Li, J. Chen, J. Zhang, H. Zheng, B. Yuan, Porous nickel oxide microflowers synthesized by calcination of coordination microflowers and their applications as glutathione electrochemical sensor and supercapacitors, Electrochim. Acta 85 (2012) 256–262.

[51] E. Frackowiak, F. Béguin, Carbon materials for the electrochemical storage of energy in capacitors, Carbon 39 (6) (2001) 937–950.

[52] S. Fang, D. Bresser, S. Passerini, Transition metal oxide anodes for electrochemical energy storage in Lithium- and sodium-ion batteries, Adv. Energy Mater. 10 (1) (2020) 1902485.

[53] A. Numan, P. Ramesh Kumar, M. Khalid, S. Ramesh, K. Ramesh, E.M. Shamsudin, Y. Zhan, P. Jagadesh, Facile sonochemical synthesis of 2D porous $Co_3O_4$ nanoflake for supercapattery, J. Alloys Compd. 819 (2020), 153019, .

[54] B. Saravanakumar, X. Wang, W. Zhang, L. Xing, W. Li, Holey two dimensional manganese cobalt oxide nanosheets as a high-performance electrode for supercapattery, Chem. Eng. J. 373 (2019) 547–555.